Naval Research Laboratory

Washington, DC 20375-5000

NRL Memorandum Report 6109

Large-Aperture Sparse Array Antenna Systems of Moderate Bandwidth for Multiple Emitter Location

W. F. GABRIEL

Electromagnetics Branch
Radar Division

November 19, 1987

SECURITY CLASSIFICATION OF THIS PAGE

REPORT DOCUMENTATION PAGE

Form Approved
OMB No. 0704-0188

1a REPORT SECURITY CLASSIFICATION UNCLASSIFIED	1b RESTRICTIVE MARKINGS
2a SECURITY CLASSIFICATION AUTHORITY	3 DISTRIBUTION/AVAILABILITY OF REPORT Approved for public release; distribution unlimited.
2b DECLASSIFICATION/DOWNGRADING SCHEDULE	
4 PERFORMING ORGANIZATION REPORT NUMBER(S) NRL Memorandum Report 6109	5 MONITORING ORGANIZATION REPORT NUMBER(S)
6a NAME OF PERFORMING ORGANIZATION Naval Research Laboratory 6b OFFICE SYMBOL (If applicable) Code 5370	7a NAME OF MONITORING ORGANIZATION
6c ADDRESS (City, State, and ZIP Code) Washington, DC 20375-5000	7b ADDRESS (City, State, and ZIP Code)
8a NAME OF FUNDING/SPONSORING ORGANIZATION Office of Naval Technology 8b OFFICE SYMBOL (If applicable) ONT	9 PROCUREMENT INSTRUMENT IDENTIFICATION NUMBER
8c ADDRESS (City, State, and ZIP Code) Arlington, VA 22217	10 SOURCE OF FUNDING NUMBERS PROGRAM ELEMENT NO: 62111N PROJECT NO: RU11W70 TASK NO: WORK UNIT ACCESSION NO:

11 TITLE (Include Security Classification)
Large-Aperture Sparse Array Antenna Systems of Moderate Bandwidth for Multiple Emitter Location

12 PERSONAL AUTHOR(S)
Gabriel, W. F.*

13a TYPE OF REPORT	13b TIME COVERED	14 DATE OF REPORT (Year, Month, Day)	15 PAGE COUNT
Interim	FROM 11/86 TO 7/87	1987 November 19	45

16 SUPPLEMENTARY NOTATION
*Sachs/Freeman Associates, Inc., Landover, MD 20735

17 COSATI CODES			18 SUBJECT TERMS (Continue on reverse if necessary and identify by block number)
FIELD	GROUP	SUB-GROUP	Antennas, Adaptive, Arrays, Emitter location, Spatial spectral analysis, Linear prediction filters

19 ABSTRACT (Continue on reverse if necessary and identify by block number)

Spatial Linear Prediction Filter (SLPF) antenna systems of large aperture width (in wave-lengths) are described for the superresolution estimation of multiple emitter locations over moderate bandwidths. To accomplish this difficult task with reasonably few degrees-of-freedom (DOF) from the large aperture, the system employs interferometer/sparse array techniques in conjunction with a shaped reference beam which may be steered to the spatial sector of interest. Computer simulations on several multiple source examples have demonstrated that the concept is feasible, provided that true time-delay steering is employed on the shaped reference beam. The optimal estimation system configuration results when time-delay steering is also applied to the interferometer elements, because this "focuses" the sample covariance matrix and minimizes the DOF required. (Even transversal filters may be dispensed with under "focused" conditions if the bandwidth is moderate.) System performance goals included high-resolution with few DOF, fast response/processing time, moderate cost, and ease of frequent calibration.

20 DISTRIBUTION/AVAILABILITY OF ABSTRACT	21 ABSTRACT SECURITY CLASSIFICATION
☒ UNCLASSIFIED/UNLIMITED ☐ SAME AS RPT ☐ DTIC USERS	UNCLASSIFIED
22a NAME OF RESPONSIBLE INDIVIDUAL William F. Gabriel	22b TELEPHONE (Include Area Code) (202) 767-2584 22c OFFICE SYMBOL Code 5370

DD Form 1473, JUN 86 *Previous editions are obsolete.* SECURITY CLASSIFICATION OF THIS PAGE

S/N 0102-LF-014-6603

CONTENTS

LARGE-APERTURE SPARSE ARRAY ANTENNA SYSTEMS OF MODERATE BANDWIDTH FOR MULTIPLE EMITTER LOCATION

I. INTRODUCTION

The application of spectral estimation techniques to resolving multiple, closely-spaced sources of significant bandwidth is a challenging problem area which has been addressed by a number of investigators [1-6]. For example, Buckley [1] utilizes linearly constrained minimum variance beamformers in which the constraints are derived from source representation spaces and are termed eigenvector constraints. His paper contains a good description of the general broadband source problem plus analyses of several approaches. Wang and Kaveh [3] proposed a coherent subspace approach to eigenvector-based broadband spatial spectral estimation in which a "focussed" matrix technique is employed, based upon approximate apriori source location information. The "focussing" corresponds to time-delay steering in broadband beamforming. Wax, Shan, and Kailath [4] utilize decomposition of the snapshot vectors into a discrete set of narrowband frequency components which are then processed independently, their null spectra superimposed, and finally inversion to form the broadband spatial spectrum.

This paper is concerned with applying a few of the above-referenced broadband concepts to a spatial linear prediction filter (SLPF) source-estimator antenna system which features a large aperture width (in wavelengths) but employs relatively few degrees-of-freedom (DOF) for accomplishing the estimations. Such a system would be a natural companion to the partially adaptive, low-sidelobe, phased array described by Gabriel

Manuscript approved August 31, 1987.

[7], deriving considerable benefit from shared hardware and data processing equipment. It is helpful to review the primary objectives that led to the investigation of this particular type of SLPF source estimator antenna system:

a. Utilize the largest antenna aperture width available in order to maximize resolution capability [8].

b. Employ interferometer/sparse array techniques to minimize the antenna hardware DOF needed, consistent with the postulated source distribution [9,10]. This objective is driven by speed of response and cost considerations.

c. Accommodate the moderate bandwidths associated with phased array radar systems [11]. This implies processing received signal samples which are correlated in both the spatial domain and the time domain. Adaptive transversal filters are often employed in such processing [1,2,12,13], but they have the inherent disadvantage of greatly increasing the number of adaptive DOF.

d. Restrict the source estimation to a narrow spatial sector that can be steered, with the sector position determined either from approximate apriori information or a deterministic search procedure. This particular sector shall be denoted as the assigned search (AS) sector.

e. Filter out or discriminate against all other sources that are located outside of the AS sector.

f. Be aminable to frequent calibration of the system by using strong sources of opportunity.

Section II develops the snapshot signal model which was utilized in conducting the investigation, and it illustrates the problem of processing

received signal samples which are correlated in both the spatial domain and the time domain over a modest RF bandwidth.

Section III discusses a constrained beamspace partially adaptive array system with an adaptive transversal filter on each beam. Here, the reader is introduced to a broadband adaptive system and becomes acquainted with dual-domain performance behavior against broadband and distributed interference sources.

Section IV then leads into our first large-aperture, interferometer-style, SLPF source estimator antenna system wherein we demonstrate the estimation of closely spaced multiple sources of moderate bandwidth. The SLPF system features an Interferometer Beamformer and a shaped AS sector "reference" beam, both of which may be steered to the AS sector of interest. A transversal filter is connected to each assigned beam port. The initial source simulation example is chosen to produce a wide equivalent spatial bandwidth spread, but yet without any significant spatial "overlap" within the common bandwidth. This example is utilized to illustrate a number of principles including: pattern shift with frequency, notch cancellation vs. source estimation, and the very effective performance of 3-tap transversal filters connected into a few beams.

Section V considers the more interesting source simulation example wherein the multiple sources have significant "overlap" of their equivalent spatial bandwidth spread and, in addition, are located so close together as to require superresolution. This example is utilized to illustrate that simple phase-shifter steering of the beams may seriously degrade estimation performance and that, at the very least, the reference beam should be steered via true time-delay. Optimal estimation performance is then demonstrated when time-delay steering is utilized on all

element signals, and it is pointed out how this represents a practical implementation of the "focussed" covariance matrix technique proposed by Wang and Kaveh [3].

It should be noted that throughout this report, source estimation is indicated by conventional spatial antenna pattern nulls. This physical graphical representation emphasizes that we are dealing with a linear prediction filter in which the null positions of the spatial filter function estimate the locations of the spatial point-sources. Reference [8] is recommended for a review of this fundamental principle, and a reminder that filter nulls can often be rather "fragile" estimates of the true spectrum.

II. SNAPSHOT SIGNAL MODEL

This signal model is developed in a tutorial manner because it is the key to understanding the behavior of our rather complex, dual-domain antenna system. Consider a linear array of K elements as shown in Fig. 1, wherein the received signal samples are correlated in both space and time. The postulated signal environment on any given observation consists of I plane waves of L spectral lines arriving from distinct spacial directions θ_i. The RF phase at the kth antenna element resulting from the ℓth spectral line of the ith source will be the product,

$$2\pi X_{k\ell} \sin\theta_i \tag{1}$$

where $X_{k\ell}$ is the location of the element phase center with respect to the midpoint of the array in wavelengths. All element phasing is referenced to the midpoint or center of the array. Note that if our elements are equally spaced by a distance, d, $X_{k\ell}$ may be written,

$$X_{k\ell} = \left(\frac{d}{\lambda_\ell}\right)\left[k - \left(\frac{K+1}{2}\right)\right] \tag{2}$$

where λ_ℓ is the RF wavelength of ℓth spectral line.

The complex amplitude of the ℓth spectral line of the ith source at the array midpoint reference is $p_i(\ell)$, such that we can express the ℓth frequency component of the nth time-sampled signal at the kth element as,

$$E_k(n,\ell) = n_k(n,\ell) + \sum_{i=1}^{I} p_i(n,\ell) g_k(\theta_i) \exp(j2\pi X_{k\ell} \sin\theta_i) \tag{3}$$

where $g_k(\theta_i)$ is the element pattern amplitude in the direction θ_i, and $n_k(n,\ell)$ is the ℓth frequency component of the nth sample from the kth element independent Gaussian receiver noise. The receiver noise is assumed to be a random process with respect to the frequency spectral line index ℓ, the time index n and the element index k. It is also assumed that the source signals are uncorrelated with receiver noise. Equation (3) permits us to construct a convenient column vector of observed data in the form

$$\underline{E}(n,\ell) = \underline{D}(\ell)\underline{p}(n,\ell) + \underline{n}(n,\ell) \tag{4}$$

where $\underline{D}(\ell)$ is a KxI matrix containing a column vector $\underline{d}_i(\ell)$ for each of the I source directions, i.e.,

$$d_{ki}(\ell) = g_k(\theta_i)\exp(j2\pi X_{k\ell} \sin\theta_i) \, . \tag{5}$$

Equation (4) separates out the basic variables of source direction in the direction matrix $\underline{D}(\ell)$, source baseband signal in the column vector $\underline{p}(n,\ell)$, and element receiver channel noise in the column vector $\underline{n}(n,\ell)$. The vector $\underline{E}(n,\ell)$ is defined as the ℓth spectral line component of the nth snapshot, i.e., a simultaneous signal sampling across all K array elements at the nth time instant. These snapshots would nominally occur at the Nyquist sampling rate corresponding to our receiver bandwidth.

The L frequency spectral line components of the source signals may be viewed as a DFT (discrete fourier transform) of the snapshots. For our simple analysis purposes, let us postulate that the spatial point source signals are uncorrelated with one another and, in addition, that the L spectral line components are uncorrelated. A total of L=21 spectral lines were utilized in the simulations, equally spaced over the RF bandwidth, and the index ℓ was stepped sequentially on each snapshot to produce "sawtooth" swept-frequency signals. Thus, the index ℓ is related to the index n,

$$\ell = n - 21\left[\mathrm{INT}\left(\frac{n-1}{21}\right)\right] \tag{6}$$

where INT(x) means the integer value of x.

To illustrate the problem of processing data which is correlated in both the frequency/time domain and the spatial domain, consider forming a uniform-illumination beam pointed in the spatial direction θ_o at band-center wavelength λ_o. For elements equally spaced by the distance d, the element weights, b_k, may be written,

$$b_k = \left(\frac{1}{\sqrt{K}}\right)\exp\left\{-j2\pi\left(\frac{d}{\lambda_o}\right)\sin\theta_o\left[k-\left(\frac{K+1}{2}\right)\right]\right\} \tag{7}$$

The output of this beam for a single point-source data vector constructed per Eq. (4) would be,

$$V(n,\ell)=[\underline{b}^t\cdot\underline{E}(n,\ell)]=p(n,\ell)[\underline{b}^t\cdot\underline{D}(\ell)]+[\underline{b}^t\cdot\underline{\eta}(n,\ell)] \tag{8}$$

where $\underline{b}$ is a column vector of beam weights and $V(n,\ell)$ is the ℓth frequency component of the nth snapshot output voltage. The term of interest is the dot product of $\underline{b}$ and $\underline{D}(\ell)$,

$$[\underline{b}^t\cdot\underline{D}(\ell)] = \sum_{k=1}^{K} b_k d_k(\ell) \tag{9}$$

Substituting from (5) and (7) we have products of the form

$$b_k d_k(\ell)=\left(\frac{g_k(\theta)}{\sqrt{K}}\right)\exp\{j2\pi[k-(\tfrac{K+1}{2})][\tfrac{d}{\lambda_\ell}\sin\theta - \tfrac{d}{\lambda_o}\sin\theta_o]\} \tag{10}$$

The two domains interact in the sine terms, which may be factored to yield the expression,

$$[\tfrac{d}{\lambda_\ell}\sin\theta - \tfrac{d}{\lambda_o}\sin\theta_o]=(\tfrac{d}{\lambda_o})[(\tfrac{f_\ell}{f_o})\sin\theta -\sin\theta_o] \tag{11}$$

where f_o is the band-center RF frequency and f_ℓ is the ℓth RF frequency within our passband.

The peak gain of the uniform-illumination beam occurs at the spatial direction angle, θ, where Eq. (11) goes to zero, i.e.,

$$(\tfrac{f_\ell}{f_o})\sin\theta = \sin\theta_o. \tag{12}$$

There are two conditions of interest here:

a. $\theta_o = 0$ deg. The beam is steered to boresight and the direction angle, θ, will remain at boresight regardless of the frequency. Boresight is defined as the spatial direction perpendicular to the linear array aperture line.

b. $\theta_o \neq 0$ deg. The beam will point in its intended steered direction, θ_o, only when $f_\ell = f_o$. Otherwise, for $f_\ell > f_o$ the beam shifts toward boresight, and for $f_\ell < f_o$ the beam shifts away from boresight.

A little thought on Eq. (10) shows that this shifting vs. frequency occurs throughout the sidelobe regions of the beam, i.e., it affects all lobes and nulls except for the boresight direction. Examples of this pattern shifting are illustrated in the following sections. The significance of off-boresight spatial direction angle shifting vs. frequency is that spatial point-sources "spread out" and appear to the array as an equivalent spatially distributed source over their bandwidths. This effect has serious ramifications in attempting to estimate the true spatial positions of point-sources, and is the dominant problem area addressed in this paper.

Finally, let us consider the outputs obtained from attaching a tapped delay line to a beam output such as $V(n,\ell)$ given in Eq. (8). The mth tap will carry the output voltage,

$$V_m(n,\ell) = V(n,\ell)\exp\left\{-j2\pi(m-1)\left(\frac{\Delta f_\ell}{f_s}\right)\right\} \qquad (13)$$

where f_s is the sampling rate and Δf_ℓ is the translated signal band spectral line corresponding to the ℓth RF frequency. The unit delay, T,

between taps is assumed to be exactly equal to the sampling period, and it is further assumed that the signal energy is band-limited by a rectangular filter to prevent "aliasing" [14].

The number of taps needed in our transversal filter may be estimated from the aperture-bandwidth product for a given source situation. Define this product as

$$B_r\left(\frac{D}{\lambda_o}\right)\sin\theta_i \tag{14}$$

where D is the total antenna aperture width, and B_r is the RF bandwidth normalized to the midband frequency. This product must be equalled by the delay-bandwidth product of the transversal filter, or

$$B_t\left(\frac{\tau}{T}\right) = B_r\left(\frac{D}{\lambda_o}\right)\sin\theta_i \tag{15}$$

where τ is the total length of the delay line and B_t is the transversal filter bandwidth normalized to the sampling rate. The value of (τ/T) then gives us the number of taps required.

III. CONSTRAINED BEAMSPACE SLC WITH A TRANSVERSAL FILTER ON EACH BEAM

The spatial/time/frequency domain adaptive performance is reviewed for a constrained beamspace sidelobe-canceller (SLC) antenna system wherein each auxiliary SLC beam feeds into a multiple-tap delay line (transversal filter). The purpose of the review is threefold: (a) to illustrate the interaction between the spatial domain and the time/frequency domain in cancelling broadband spatial point-sources; (b) to illustrate the special problem area encountered when spatially distributed sources are involved; and (c) to become acquainted with an adaptive SLC

antenna system which utilizes similar principles of operation and would constitute a natural application area for the postulated source estimation processor.

Figure 2 illustrates a schematic diagram of the particular type of partially adaptive array system under discussion. It consists of two beamformer subsystems which connect into common array aperture elements. The use of common elements helps to avoid polarization problems in the adaptive nulling performance. The mainbeam subsystem (on the left-hand side in Fig. 2) is intended to function as a conventional low-sidelobe phased array capable of electronic scan over the region of interest. Sidelobe level is determined by the usual quality of the elements, phase shifter modules, and corporate feed. The second beamformer subsystem is intended to furnish a set of SLC beams for selective subtraction from the mainbeam. Thus, it is referred to as the SLC subsystem. This SLC subsystem is auxiliary to the mainbeam subsystem and consists of a beamformer which is coupled into the aperture at the elements, prior to the TR module phase shifters. This beamformer does not require low-sidelobe design and may consist of either a Butler matrix type or a lens type such as a Rotman lens. A very favorable feature from the standpoint of potential bandwidth is that all beams have the same phase center, i.e., the geometric center of the array aperture. Orthogonality in the family of beams is desirable but need not be precise for our purposes.

The output beam ports connect into a "Beam Assignment Selector" wherein they are electronically switched into the SLC algorithm processor based upon source location estimates. The idea is to connect in only enough SLC beams to cancel a given source distribution situation, thus minimizing sidelobe degradation. The general principles of beamspace SLC

have been described in the literature [7] and shown to offer advantages of a stable mainbeam, retention of low sidelobes, very fast adaptive response, and no adaptive grating lobes.

Each of the selected beams feeds into a tapped delay line, usually referred to as a transversal filter. It is this latter arrangement that permits adaptivity in the time/frequency domain [13,15,16] in addition to adaptivity in the spatial domain. The transversal filter (TF) output taps then feed into the black box labelled "SLC Algorithm Signal Processor", which applies an adaptive algorithm to obtain the TF tap weights for achieving cancellation. This type of system is amenable to any of the current adaptive processing algorithms, including even analogue versions.

Two different interference scenarios were selected for illustrating the cancellation performance of the Fig. 2 SLC antenna system; spacial point-source of broad bandwidth, and spatially distributed interference sources. These were evaluated via computer simulations which utilized a 16-element linear array with half-wavelength element spacing as the common aperture. The mainbeam subsystem was given a quiescent Taylor illumination taper designed for 30 dB sidelobes, and the SLC subsystem beamformer was chosen to be a Butler Matrix type. Figure 3 shows a plot of a typical quiescent pattern for this array, with the mainbeam steered to -15 degrees. The adaptive weights for the two scenarios were computed from the sample covariance matrix inverse (SMI) algorithm [7].

a. **Spacial Point-Source With Bandwidth**

This simulation involved a single 33 dB point-source located at +44 degrees azimuth, with the bandwidth parameter varied. A single beam, No. 14, from the Butler matrix SLC beamformer was assigned to cover this point-source. Cancellation performance for this single beam was evaluated

with and without a transversal filter. Figure 4 is a plot of typical adapted patterns with a 3-tap transversal filter at the low, midband, and high frequencies of the 10 percent RF bandwidth example. Note the considerable shift in the sidelobes versus frequency, but yet the null remains steady at the location of the point-source. Figure 5 then shows a summary of performance for this case, where we plot the adapted output in dB above receiver noise level versus the percent RF bandwidth multiplied by $\sin(\theta_i)$, where θ_i is the angular location of the point-source. Note that the performance of the SLC beam plus a transversal filter is much superior to the SLC beam alone, which indicates that the extra DOF's from the transversal filter taps are providing effective adaptivity in the frequency domain to cancel the broadband interference.

The curves in Fig. 5 are dependent upon the location of the point-source with respect to both the mainbeam sidelobes and the auxiliary SLC beam. Thus, they may be used only for qualitative comparison purposes.

b. **Spatially Distributed Interference**

This simulation involved eleven 40 dB sources distributed uniformly in angle about the center position of +44 degrees azimuth, with the angular width parameter varied. Beams Nos. 13, 14, and 15 from the Butler matrix SLC beamformer were assigned to cover this distributed interference. These beams are illustrated in Fig. 6. Cancellation performance was evaluated with and without a transversal filter on each beam. Figure 7 illustrates a typical adapted pattern for the example wherein the eleven sources were distributed over a sector width equal to 1.25 beamwidths. Note that the three beams readily handle this rather wide angular distribution of interference. Figure 8 then shows a summary of performance for this scenario, where we plot the adapted output power in dB above

receiver noise level versus the distributed sector width in beamwidths, for one, two and three SLC beams. Note the considerable increase in performance obtained by utilizing three beams instead of just one or two.

A significant observation from these simulation runs was that the addition of a transversal filter on each beam had virtually no effect on the cancellation performance, i.e., the extra DOF's from the transversal filter taps did not provide any additional adaptivity in the spatial domain to counter distributed interference. The curves in Fig. 8 are dependent upon the location of the distributed interference with respect to both the mainbeam sidelobes and the auxiliary SLC beams. Thus, they may be used only for qualitative comparison purposes.

The SLC system of Fig. 2 has also been found to be very effective in the cancellation of delayed multipath signals which get into the mainbeam (time domain adaptivity) [15] and the cancellation of channel mismatch errors (frequency domain adaptivity within the receiver system passband [16].

IV. A SHAPED BEAM SLPF ESTIMATOR WITH TF

Building upon the introductory material of the previous sections, we now proceed to large-aperture interferometer/sparse array techniques and evaluate their estimation performance against closely-spaced multiple sources of moderate bandwidth. The particular type of SLPF source estimator antenna system under investigation is shown in Fig. 9. Aperture width was chosen to be 25λ (wavelengths) midband, which would accommodate 49 elements of half-wavelength spacing, if filled. From this aperture, we select nine (9) elements, spaced 3λ apart, which feed their signals thru a phase shifter into an interferometer beamformer. The purpose of the phase shifters is to permit steering the beamformer beams to an assigned search

(AS) spatial sector. For example, Fig. 10 illustrates a typical midband cluster of 9 beams formed by a Butler Matrix beamformer and steered to an azimuth center position of 42°. The details of the interferometer beamformer weights are contained in Appendix A, where it is noted that the cluster is not unique and will replicate itself several times throughout visible space because of the wide element spacing of 3λ.

The output beam ports connect into a "Beam Assignment Selector" wherein they are electronically switched into a few transversal filters (TF) in a manner similar to the Fig. 2 system. The TF output taps then feed into the SLPF Algorithm Signal Processor. In this manner, we funnel down to the few DOF that will be utilized in performing source estimation over a moderate bandwidth. The number of TF taps is selectable.

A final similarity between Fig. 9 and Fig. 2 is that a "mainbeam" is included, albeit of much different characteristics. For source estimation, we desire a shaped beam, hereafter denoted as the AS sector reference beam, which is of constant gain across the AS sector, but of low sidelobe level elsewhere. In other words, the ideal reference beam would be a rectangular-shape which passes the AS spatial sector but filters out all sources which are located outside it. Figure 11 illustrates the particular reference beam that was utilized for the simulations contained in this report. It is based upon a 19-element filled linear array whose phase center is located 7.5λ away from the phase center of the interferometer beams, and which can be electronically steered to the AS sector of interest. The phase center of the reference beam must be separated significantly from the phase center of the interferometer beamformer in order to achieve robust spatial estimation performance. Details of the reference beam element weights are contained in Appendix A.

Equation Formulation

An equation formulation for the SLPF antenna/processor system of Fig. 9 may be developed in terms of the same pattern subtraction principles as utilized for the similar beamspace partially adaptive array system of reference [7], where the optimum adaptive weight column vector, $\underline{W}_o$, was expressed for K beamformer beams as,

$$\underline{W}_o = \underline{S}^* - \sum_{k=1}^{K} W_k \underline{b}_k \tag{16}$$

where $\underline{S}^*$ is a column vector of the element weights associated with the AS sector reference beam, $\underline{b}_k$ is the kth Butler Matrix beamformer beam column vector of element weights, and W_k is the adaptive weight applied to the kth beam. The solution for W_k may be arrived at via any of the current adaptive processing algorithms, recognizing that there are performance differences.

Pointing toward the sample matrix inverse (SMI) algorithm, we take advantage of the fact that our sample covariance matrix of signal inputs, $\hat{\underline{R}}$, involves only the J assigned beams needed, and its dimensions reduce from KxK down to JxJ, thereby easing the computation burden involved in obtaining its inverse [13]. The equivalent "steering vector" $\underline{\Lambda}$ per Applebaum [17] is also reduced to dimension J and consists of the cross-correlation between the reference beam signal V and J assigned beam outputs $\underline{Y}$,

$$\underline{\Lambda} = \frac{1}{N} \sum_{n=1}^{N} V(n,\ell)\underline{Y}^*(n,\ell) \tag{17}$$

where N is the number of snapshots and index ℓ is related to n (see Eq. (6)). The jth assigned beam output for the nth snapshot signal sample is simply

$$Y_j(n,\ell) = (\underline{E}^t(n,\ell)\cdot\underline{b}_k),\ k \text{ set by } j \tag{18}$$

where $\underline{E}(n,\ell)$ is the signal snapshot vector described in Section II, and the particular beam index k must be selected for the jth assigned beam. $V(n,\ell)$ is the ℓth frequency component of the nth snapshot output voltage of the reference beam, computed from

$$V(n,\ell) = (\underline{E}^t(n,\ell)\cdot\underline{S}^*). \tag{19}$$

Our J dimension adaptive weight solution thus becomes,

$$W = [\hat{\underline{R}}^{-1}\underline{\Lambda}] \tag{20}$$

where

$$\hat{\underline{R}} = \frac{1}{N}\sum_{n=1}^{N}[\underline{Y}(n,\ell)\underline{Y}^{*t}(n,\ell)]\ . \tag{21}$$

Finally, if transversal filters with M taps are being used, then the beam output snapshot vector becomes a partitioned or stacked vector of M segments, i.e.,

$$\underline{Y}^t(n,\ell) = [\underline{Y}_1^t(n,\ell) \mid \underline{Y}_2^t(n,\ell) \mid \cdots \mid \underline{Y}_M^t(n,\ell)] \tag{22}$$

wherein the vector components are defined as in Eq. (13), and the above expressions must be modified to accommodate the partitioned matrices.

Needless to say, the matrix dimensions are greatly increased when the transversal filters are employed, thus substantially increasing computation burden.

Estimating Multiple Sources With No "Overlap"

The first estimation example to be presented involves a simulation in which we have three 16.7 dB spatial point-sources of 10% swept RF bandwidth, located at 37, 42, and 48 degrees azimuth. These parameters were deliberately chosen so that there would be a continuous "equivalent" spatial interference distribution spread* over the rather wide angular region extending from about 35° to 51.5° azimuth (roughly 5 beamwidths in extent), but yet without any significant equivalent spatial overlap within their bandwidths. To graphically demonstrate the importance of the transversal filters, our first estimation pattern was run with no TF present. All nine beams from the interferometer beamformer were utilized, thus giving us a $\hat{\underline{R}}$ matrix dimension of 9. Also, both the AS sector reference beam and the Interferometer Beamformer were phased-steered to a center position of 42° azimuth as shown in Figs. 10 and 11.

The sample covariance matrix $\hat{\underline{R}}$ and the steering vector $\underline{A}$ (Eqs. (17) and (21) were accumulated and averaged over a total N=1260 snapshots. The resultant adaptive weights $\underline{W}$ computed from Eq. (20) then give us the spatial pattern source estimate shown in Fig. 12(a). Several comments are in order regarding this adaptive pattern:

a. There is no spatial spectrum estimate per se because, with no TF present, the array processor cannot separate the two domains. It "sees" a

---

* See Section II for an explanation of equivalent spatial bandwidth spread.

distributed source and utilizes its 9 DOF to form a wide spatial filter cancellation notch.

b. The adaptive pattern is shown plotted at three different frequencies within the 10% bandwidth: lowest, midband, and highest. Note that for $f_\ell > f_o$ the pattern shifts toward boresight, and for $f_\ell < f_o$ the pattern shifts away from boresight. Recall the discussion in Section II.

c. This performance is identical to what we would get if the processor operated from the 9 interferometer element signals directly, i.e., the beamformer operation is a linear transformation of the element signals.

d. It demonstrates the same principle of distributed source notch cancellation as shown in Fig. 7 for the SLC system.

e. The eigenvalues computed for the particular $\hat{\underline{R}}$ of this case, normalized to unity receiver noise power level, were: 186.1, 160.0, 151.3, 128.4, 112.9, 86.1, 24.0, 2.8, and 1.1. Note that there are eight unique eigenvalues represented here.

Next, the same case was run with the TF included, but with fewer beams. Beams Nos. 3,4,5,6 and 7 from the Interferometer Beamformer were assigned to cover this source situation, with a 3-tap TF selected for each of the five beams. Thus, our matrix dimension for data processing is now 15, and we must incorporate partitioned vectors per Eq. (22). The resultant adaptive weights spatial patterns are shown in Fig. 12(b) where we note the following points:

a. There is now a valid spatial spectrum estimate indicated by the rather consistent positioning of three nulls in the adapted patterns, shown plotted at three frequencies within the 10% bandwidth.

b. Despite the considerable equivalent bandwidth spread, the 3-tap TF permit separation of the frequency/time domain from the spatial domain

in this case. Note the absence of pattern shifting as compared to Fig. 12(a).

c. This is an excellent illustration of a fundamental difference between source estimation and source cancellation systems. Both systems filter source signals out of their outputs, but in the former case, we desire that the filtering be performed via reasonably distinguishable nulls located at the source positions - a much more difficult task.

d. The eigenvalues computed for the particular $\hat{\underline{R}}$ of this case, normalized to unity receiver noise power level, were: 469.6, 407.5, 288.7, 275.7, 229.1, 189.1, 157.7, 82.8, 38.5, 33.0, 9.3, 1.7, 1.6, 1.3, and 1.1. Note that there are about 11 unique eigenvalues represented here.

V. ESTIMATING MULTIPLE SOURCES WITH SIGNIFICANT "OVERLAP"

We now consider the more interesting case of estimating closely spaced multiple sources of moderate bandwidth wherein significant equivalent source overlap exists within their bandwidths. Our test simulation example was formulated by using the same three 16.7 dB spatial point-sources of 10% swept bandwidth discussed in the previous section, but moving them closer together to locations of 40, 42, and 44 degrees azimuth. Since our aperture beamwidth is 3.1 degrees at these off-boresight locations, there is the added challenge of superresolution, i.e., attempting to resolve multiple sources which are separated by less than a beamwidth.

The SPLF processor sytem conditions are the same as for Fig. 12(b) wherein both the AS sector reference beam and the Interferometer Beamformer are phase-steered to a center position of 42° azimuth as shown in Figs. 10 and 11. Also, five beams, Nos. 3, 4, 5, 6, and 7, are assigned to cover the source situations with a 3-tap TF selected for each of the

five beams. The resultant adaptive weights spatial patterns are shown in Fig. 13(a) where we note the formation of a good cancellation filter notch for the three sources, but no valid spatial spectrum estimate.

The failure to resolve the sources is caused by two factors which were simultaneously present: (a) equivalent spatial domain overlap within the common bandwidth, and (b) the AS sector reference beam undergoes both pattern shifting and phase-center shifting vs. frequency. The estimator system with TF can tolerate one of these factors at a time, as in Fig. 12(b), but not both. To demonstrate this point with the second option, let us next remove the equivalent source shifting in the AS sector reference beam by employing true time-delay steering instead of phase-steering.

Time-delay steering produces element weights which vary with frequency. Recalling the discussion in Section II, it is readily seen that Eq. (7) would become

$$b_k(\ell) = \left(\frac{1}{\sqrt{K}}\right)\exp\left\{-j2\pi\left(\frac{d}{\lambda_\ell}\right)\sin\theta_o\left[k-\left(\frac{K+1}{2}\right)\right]\right\} \qquad (23)$$

where we note the frequency dependence thru λ_ℓ. Substituting this change into Eq. (10), we see that there would be no beam shifting vs. frequency in the steering direction θ_o. Furthermore, the shifting will remain minimal for directions within a beamwidth of θ_o, provided the RF bandwidth is modest. Appendix A contains pattern plots of the AS sector reference beam for both phase-steering and true time-delay steering to a center position of 42° azimuth.

This "fixing" or stabilization of the multiple swept sources in the reference beam can be better appreciated via close examination of Eq. (17)

in the previous Section IV, where we see that the equivalent steering vector, $\underline{A}$, consists of the cross-correlations between the reference beam signals, $V(n,\ell)$, and the interferometer beam outputs $\underline{Y}(n,\ell)$. Obviously, if the sources remain constant in the $V(n,\ell)$ signal with respect to the interferometer array phase center, then all of the amplitude/phase variations vs. frequency will be confined to the interferometer beam outputs and can be compensated for by the adaptive transversal filters. Figure 13(b) demonstrates the effective compensation by the TF under this condition wherein the reference beam is steered via true time-delay rather than via phase shifters. Note that we now have a valid superresolution spatial spectrum estimate of the multiple swept-bandwidth, "overlapped" sources and, furthermore, that there is very little pattern shifting throughout the entire AS sector (compare against Fig. 12(b)).

The eigenvalues computed for the particular $\hat{\underline{R}}$ of this case, normalized to unity receiver noise power level, were: 648.7, 551.7, 403.2, 365.4, 199.4, 125.2, 80.5, 45.8, 34.1, 16.4, 6.2, 2.9, 2.4, 1.2, and 1.0. Note that there are 13 unique eigenvalues represented here.

Utilizing Time-Delay Steering on All Element Signals

If it is beneficial to minimize beam shifting of the AS sector reference beam by employing time-delay steering, then it should be even more beneficial to extend this characteristic to the Interferometer Beamformer as well by utilizing time-delay steering on all element signals. This does indeed prove to be the case for our SLPF estimator/processor system, and we end up with a practical manifestation of the "focussed" covariance matrix technique proposed by Wang and Kaveh [3]. Essentially, the time-delay steering minimizes equivalent spatial bandwidth spread to such a small value within the AS sector that transversal filters are not

really needed (assuming modest RF bandwidths). This benefit is demonstrated in Fig. 14(a) where we plot typical adapted patterns using time-delay steering on all element signals, with no transversal filters present. All nine interferometer beams were used, thus giving us a $\hat{\underline{R}}$ matrix dimension of 9, and the total number of snapshots averaged was N = 315.

The most remarkable feature about this technique is that we are getting an estimation performance fully equal to the performance demonstrated in Fig. 13, but with only 3 DOF needed as compared to 13 for the TF configuration. The DOF information is contained in the eigenvalues, which computed for the particular $\hat{\underline{R}}$ of this case as: 400.3, 345.9, 101.8, 1.4, 1.2, 1.1, 1.0, 0.95, and 0.91. Note that there are only 3 unique eigenvalues represented here, which also happens to be the minimum number associated with three spatial point-sources. This clearly indicates a "focussed" covariance matrix and would permit us to reduce the matrix dimension down to 3 DOF, i.e., only three assigned beams for this particular case. Additional benefits include fewer data snapshots required and faster speed of response.

Time-delay steering to a narrow AS sector is a fundamental technique for separating the spatial domain from the frequency/time domain. When combined with a shaped AS sector reference beam, it functions in much the same manner as a narrowband filter in the frequency domain, i.e., either technique can separate the two domains within the limitations of their "passbands" and "sidelobe levels". To illustrate this point, the final simulation example deliberately includes two additional 20 dB sources of 10% swept bandwidth located at -13.5 and -12.2 degrees azimuth. Referring to Fig. 11, note that these sources will suffer at least 24 dB of attenuation in the reference beam sidelobes and, therefore, will contribute very

little to the cross-correlated steering vector $\underline{A}$ of Eq. (17). In addition, they undergo an equivalent spatial spreading because they are about 55 degrees away from the time-delay steering direction of 42°. The resultant adapted patterns are shown in Fig. 14(b) where we note only secondary disturbances due to the two extra swept sources. If significant correlation were present, there would be a cancellation notch extending over the indicated aliased region.

An interesting aspect of this particular case is that the two extra swept sources are presented at full gain in some of the Interferometer Beamformer beams because of the wide element spacing of $3\lambda_o$, i.e., we have replication of the set of beams in Fig. 10 throughout visible space. This effect is threefold:

a. They contribute terms of high power level in $\hat{\underline{R}}$.

b. They increase and dominate the eigenvalues, which were computed as: 703.6, 575.8, 419.5, 388.1, 287.6, 192.2, 35.3, 2.3, and 1.1. Note that there are now 8 unique eigenvalues instead of 3.

c. They have an equivalent spatial bandwidth spread in the AS sector because of the aliasing from their actual location. This equivalent spread is indicated in Fig. 14(b).

The aliasing intrusion into our AS sector can be harmful if it overlaps true sources in the sector, because then the adapted weights will be affected by the extra signal power coming from "common" directions, and it may be sufficient to distort or even destroy the null in those directions.

VI. CONCLUSIONS

We have investigated the concept of performing SLPF source estimation in a narrow, steerable, spatial sector by utilizing a large antenna aperture width (in wavelengths), but requiring relatively few DOF from it

via operation in an interferometer beamformer space. Our objectives included high-resolution, the accommodation of moderate bandwidths, fast response time, moderate cost, and ease of frequent calibration. Computer simulations on several multiple-source examples have demonstrated that the concept is indeed feasible, provided true time-delay steering can be employed on the AS sector reference beam. This provision retains a reasonably stable spatial reference for each source within the sector over the common bandwidth.

The optimum estimation system results when time-delay steering can be applied to all element signals, i.e., including the interferometer elements, because this "focusses" the sample covariance matrix for sources which are within the AS sector and minimizes the DOF required. Even the transversal filters may be dispensed with under "focussed" conditions if the bandwidth is modest. When combined with a shaped AS sector reference beam, this technique functions in much the same manner as a narrow band filter in the frequency domain, i.e., it separates the spatial domain from the frequency/time domain within the limitations of its "passband" and sidelobe levels.

VII. REFERENCES

1. K.M. Buckley, "Spatial/Spectral Filtering with Linearly Constrained Minimum Variance Beamformers," IEEE Trans. ASSP, Vol. 35, pp. 249-266, Mar 1987.

2. K.M. Buckley and L.J. Griffiths, "Direct Broadband Array Data Processing for Source Location Estimations," Proc. of the Third ASSP Workshop on Spectrum Estimation and Modelling, Nortneastern University, Nov 1986.

3. H. Wang and K. Kaveh, "Coherent Signal-Subspace Processing for the Detection and Estimation of Angles of Arrival of Multiple Wide-Band Sources," IEEE Trans. ASSP, Vo. 33, pp. 823-831, Aug 1985.

4. M. Wax, T. Shan, and T. Kailath, "Spatio-Temporal Spectral Analysis by Eigenstructure Methods," IEEE Trans. ASSP, Vol. 32, pp. 817-827, Aug 1984.

5. G. Su and M. Morf, "The Signal Subspace Approach for Multiple Wideband Emitter Location," IEEE Trans. ASSP, Vol. 31, pp. 1502-1522, Dec 1983.

6. S. Nawab, F. Dowla, and R. Lacoss, "Direction Determination of Wideband Signals," IEEE Trans. ASSP, Vol. 33, pp. 1114-1122, Oct 1985.

7. W.F. Gabriel, "Using Spectral Estimation Techniques in Adaptive Processing Antenna Systems," IEEE Trans. Antennas and Propagation, Vol. AP-34, pp. 291-300, Mar 1986.

8. W.F. Gabriel, "Spectral Analysis and Adaptive Array Superresolution Techniques," Proc. IEEE, Vol. 68, pp. 654-666, Jun 1980.

9. J. Capon, "High-Resolution Frequency-Wavenumber Spectrum Analysis," Proc. IEEE, Vol. 57, pp. 1408-1418, Aug 1969.

10. R.O. Schmidt and R.F. Franks, "Multiple Source DF Signal Processing: An Experimental System," IEEE Trans. AP, Vol. 34, pp. 281-290, Mar 1986.

11. M. Skolnik, Radar Handbook, McGraw-Hill Book Co., NY, 1970.

12. L.E. Brennan, J.D. Mallett, and I.S. Reed, "Adaptive Arrays in Airborne MTI Radar," IEEE Trans. Antennas and Propagation, Vol. AP-24, pp. 607-615, Sep 1976.

13. R.A. Monzingo and T.W. Miller, "Introduction to Adaptive Arrays, Wiley, NY, 1980.

14. A.V. Oppenheim and R.W. Schafer, Digital Signal Processing, Prentice Hall, Englewood Cliffs, NJ, 1975.

15. W.F. Gabriel, "Constrained Beamspace Sidelobe Canceller (SLC) with a Tapped Delay Line on Each Beam," NRL Memorandum Report No. 6042, (in process of publication).

16. W.F. Gabriel, "Adaptive Digital Processing Investigation of DFT (Discrete Fourier Transform Subbanding vs. Transversal Filter Canceller," NRL Report No. 8981, Jul 1986. (AD-A171 894)

17. S.P. Applebaum, "Adaptive Arrays," IEEE Trans. Antennas and Propagation, Vol. AP-24, pp. 585-598, Sep 1976.

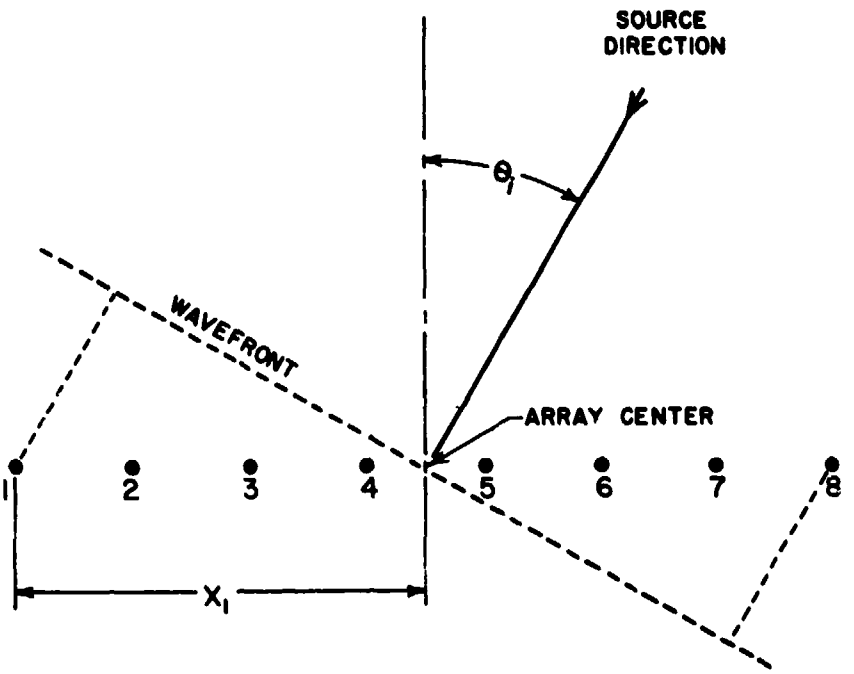

Fig. 1 — Geometry of linear array and signal wavefront

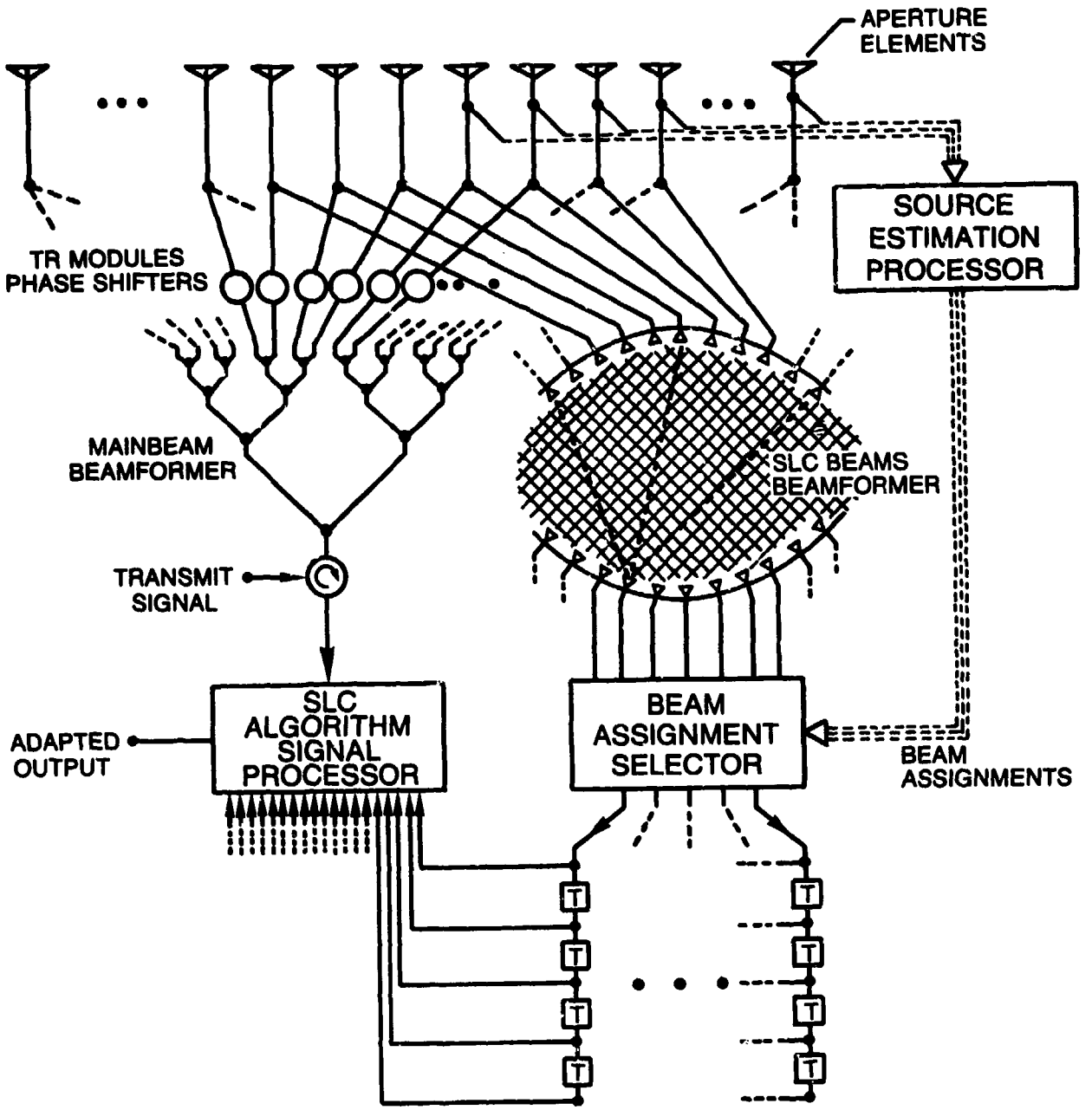

Fig. 2 — Schematic diagram of constrained beamspace SLC system with a tapped delay line on each assigned beam

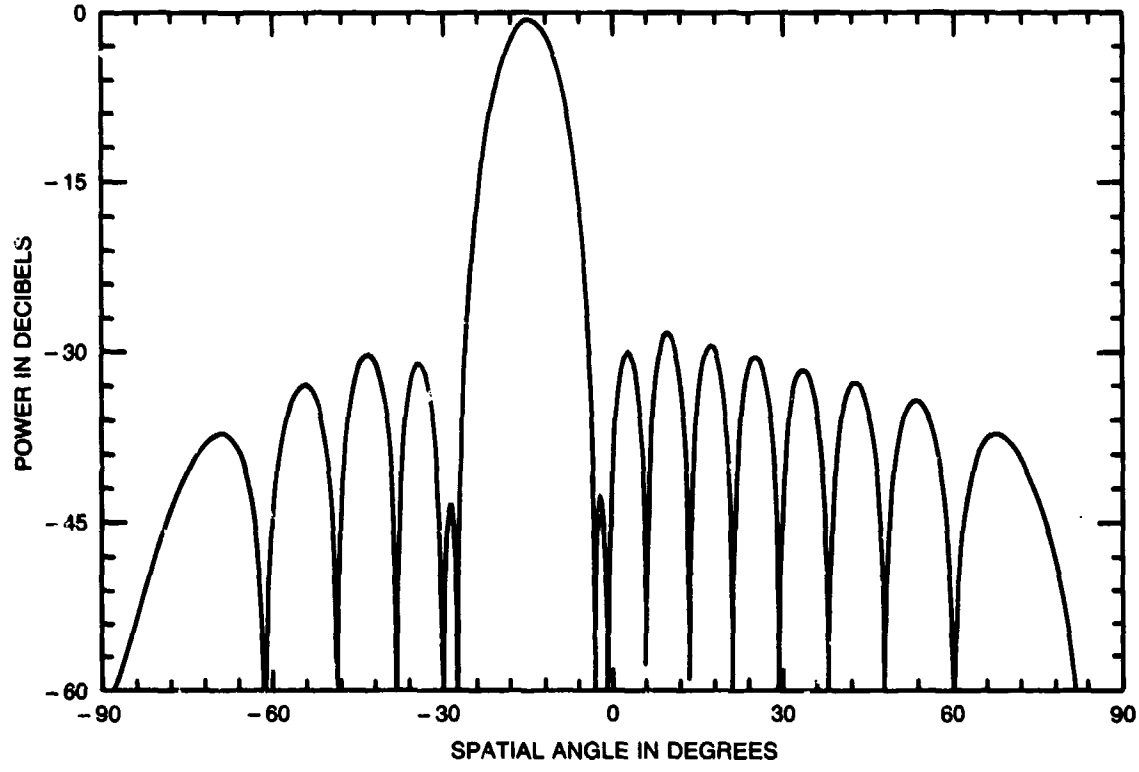

Fig. 3 — Quiescent mainbeam pattern, 16 element linear array with 30 dB Taylor illumination taper.

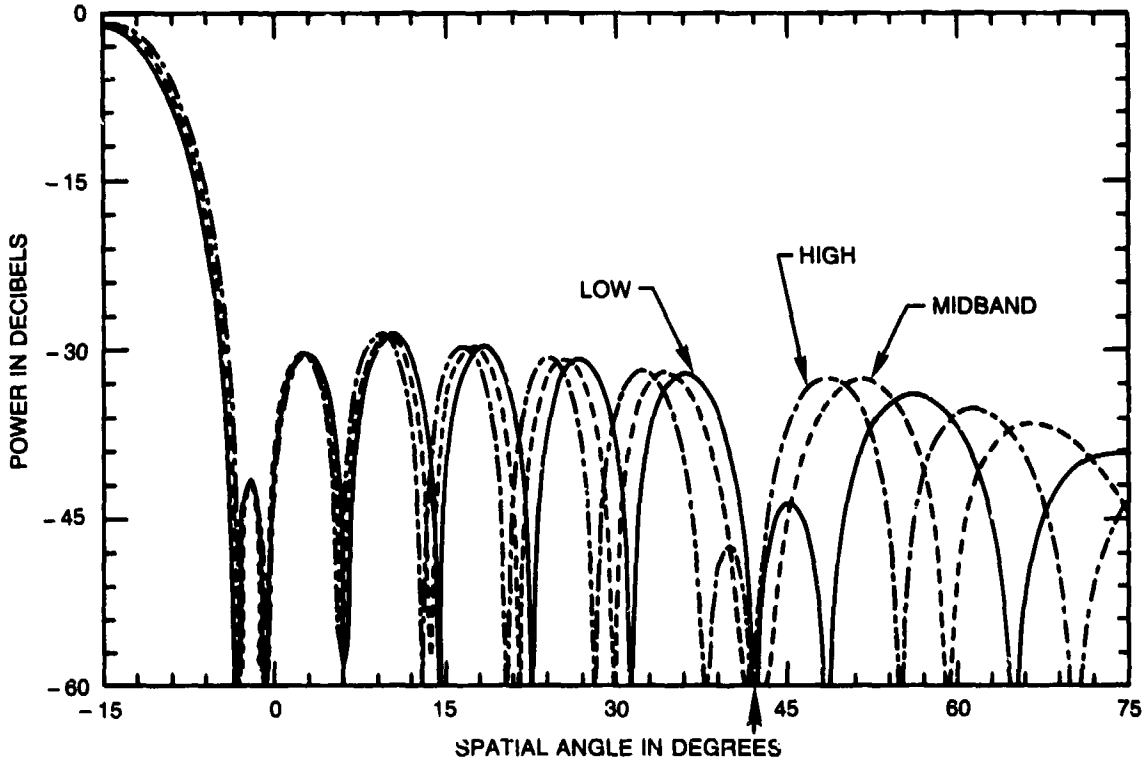

Fig. 4 — Typical adapted patterns at low, midband, and high frequency for a single 46 dB point-source located at 42 degrees, swept RF bandwidth of 10 percent; single SLC beam No. 14 with 3 tap transversal filter.

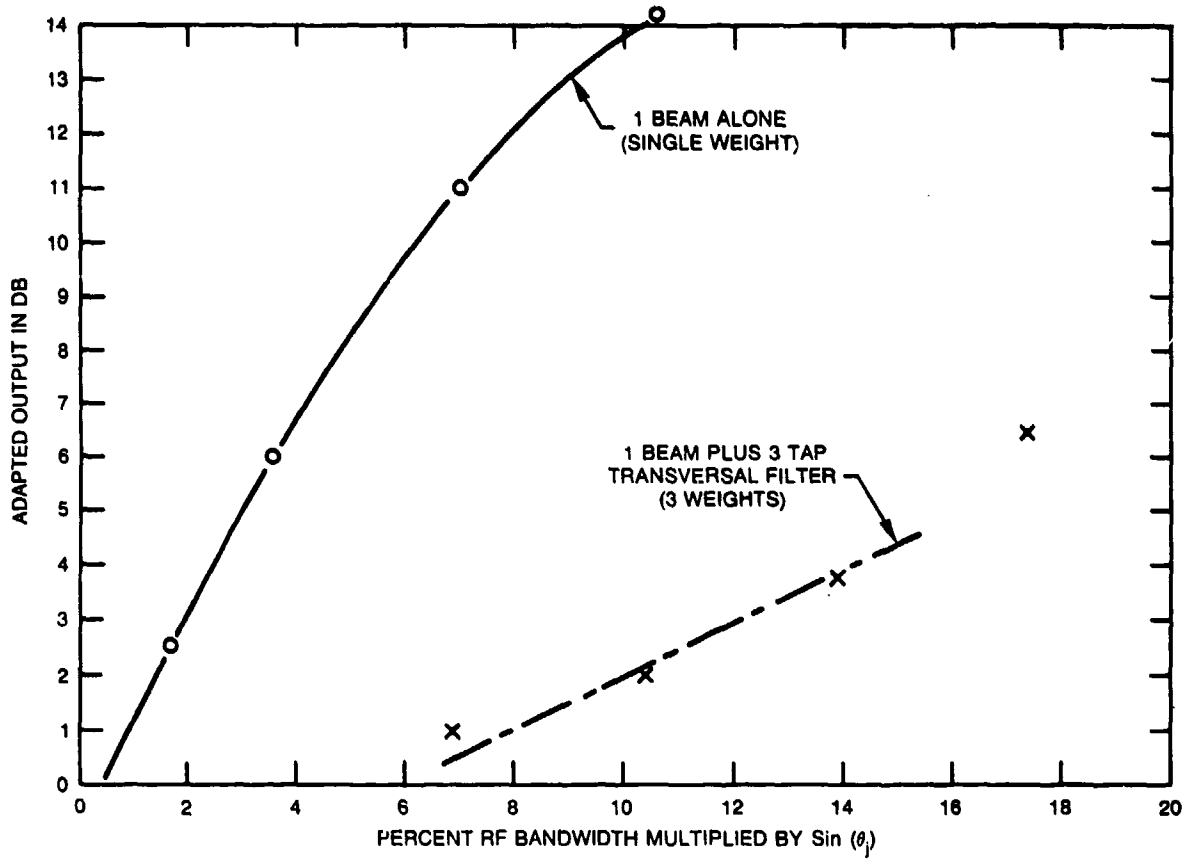

Fig. 5 — Summary of adaptive cancellation performance versus bandwidth for a single 46 dB point-source located at 44 degrees; single SLC beam No. 14.

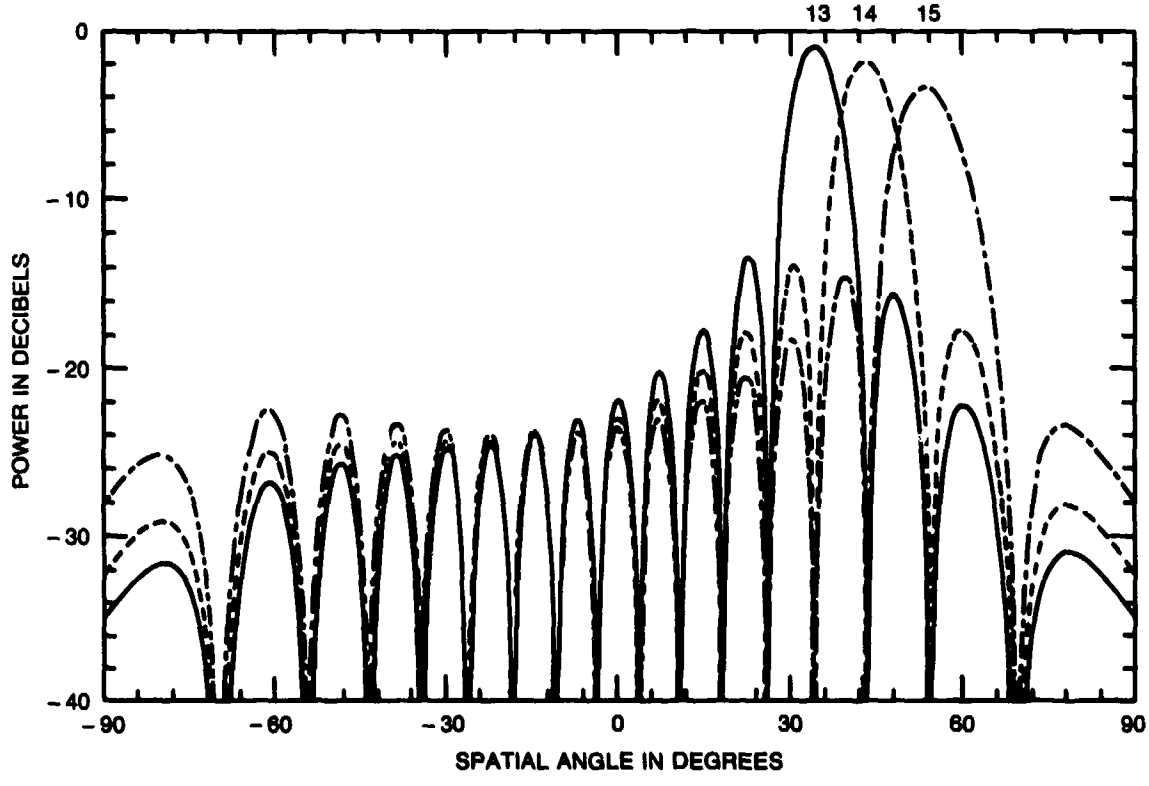

Fig. 6 — Auxiliary SLC beams Nos. 13, 14, and 15 from Butler Matrix Beamformer.

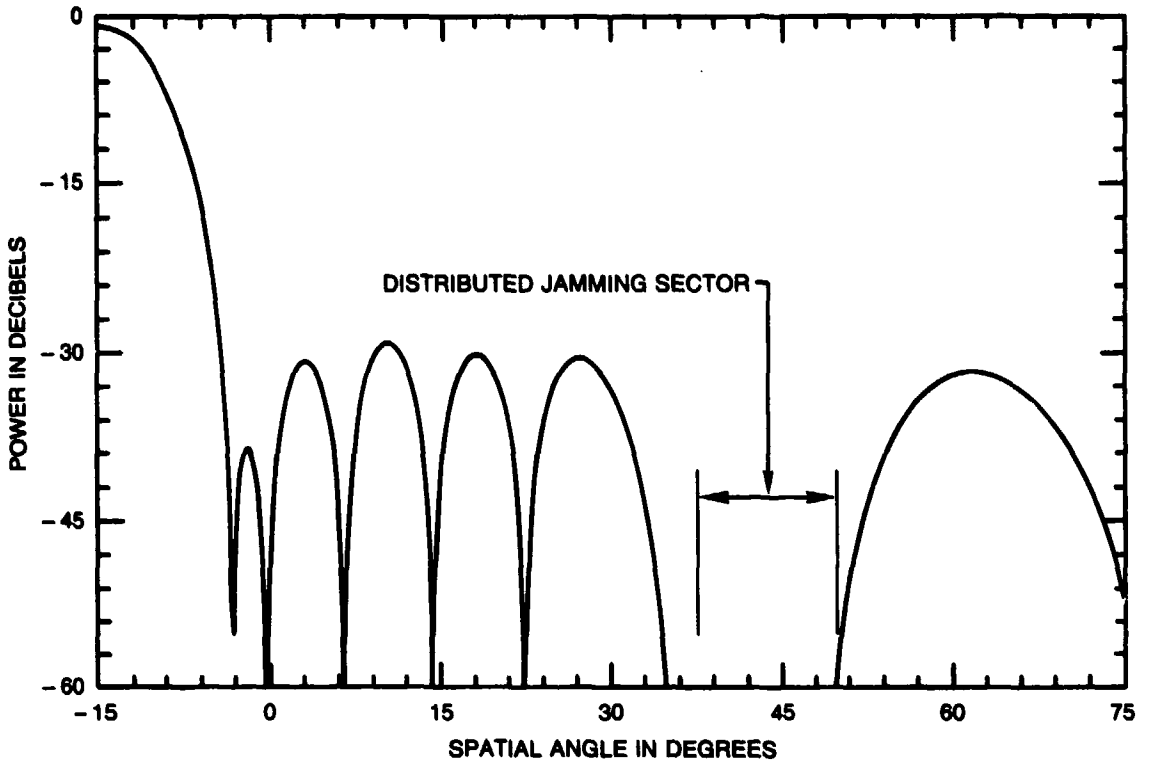

Fig. 7 — Typical adapted pattern response for eleven 40 dB sources distributed uniformly over spatial sector width of 1.25 beamwidths (37.7 to 50.2 deg.); three SLC beams Nos. 13, 14, and 15 without transversal filters.

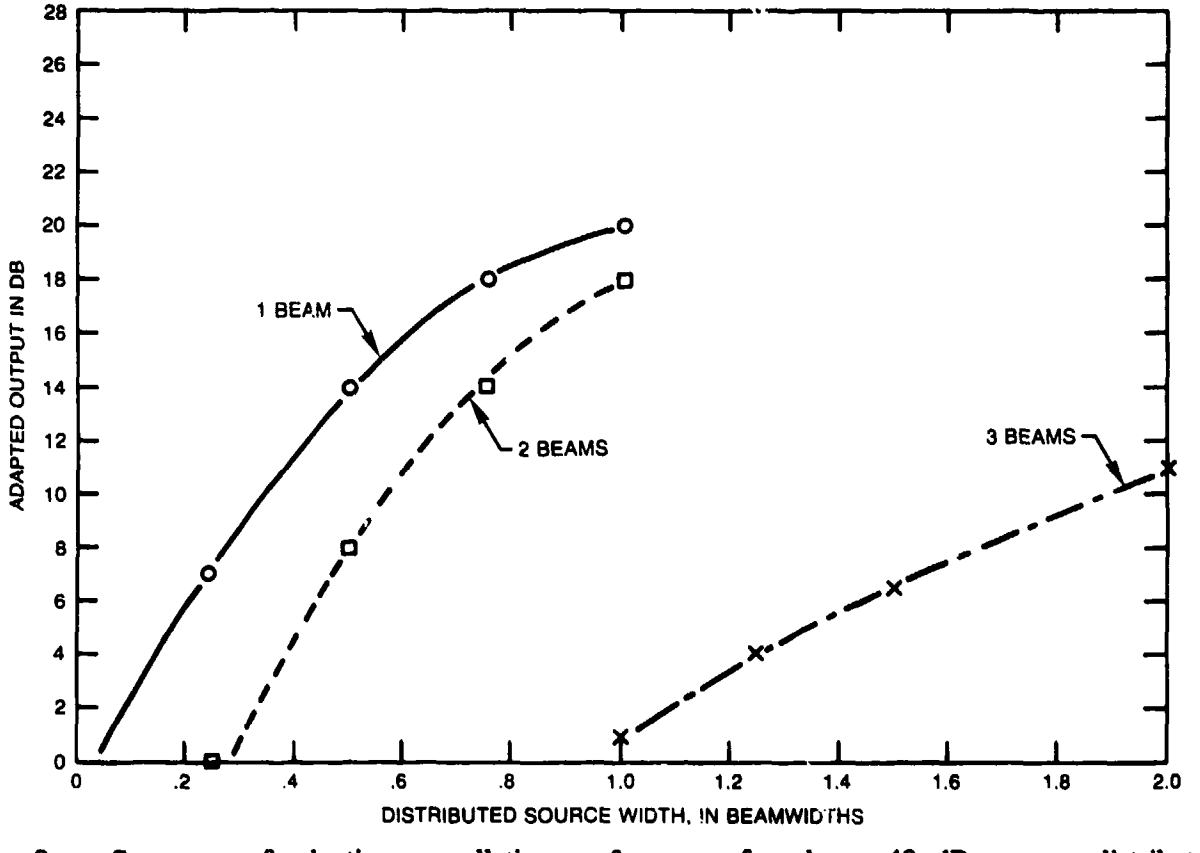

Fig. 8 — Summary of adaptive cancellation performance for eleven 40 dB sources distributed uniformly over a spatial sector; utilizing one, two, or three auxiliary SLC beams without transversal filters.

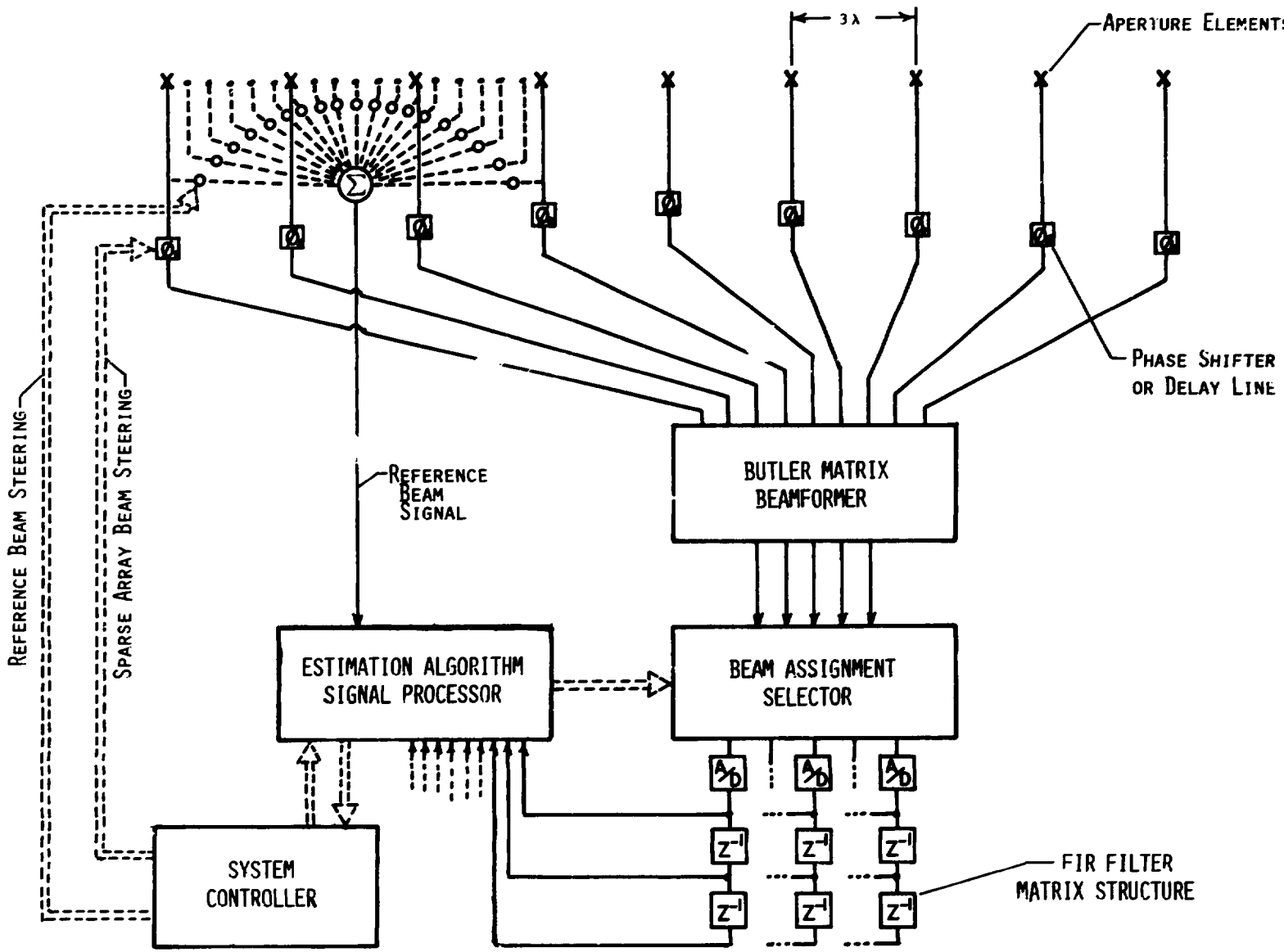

Fig. 9 — Schematic diagram of a SLPF Estimator incorporating a Sparse-Array Beamformer, a shaped Reference Beam, and a Transversal Filter structure.

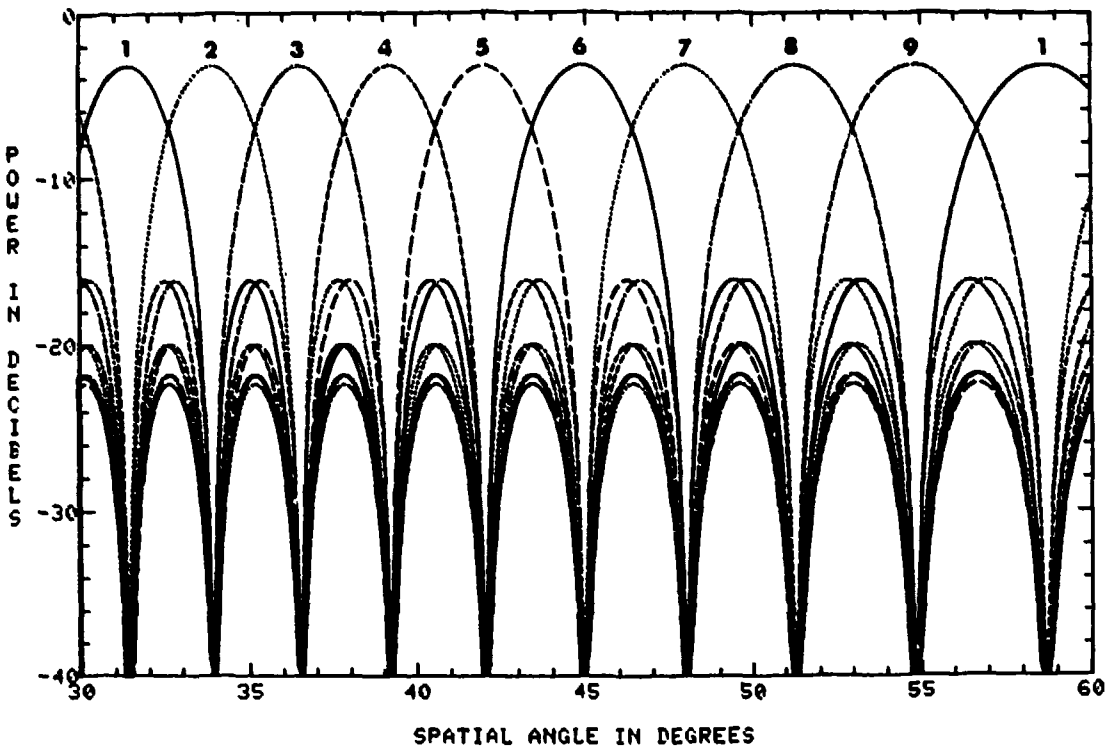

Fig. 10 — Midband cluster of 9 beams formed by Butler Matrix Interferometer Beamformer, steered to a center position of 42 degrees azimuth.

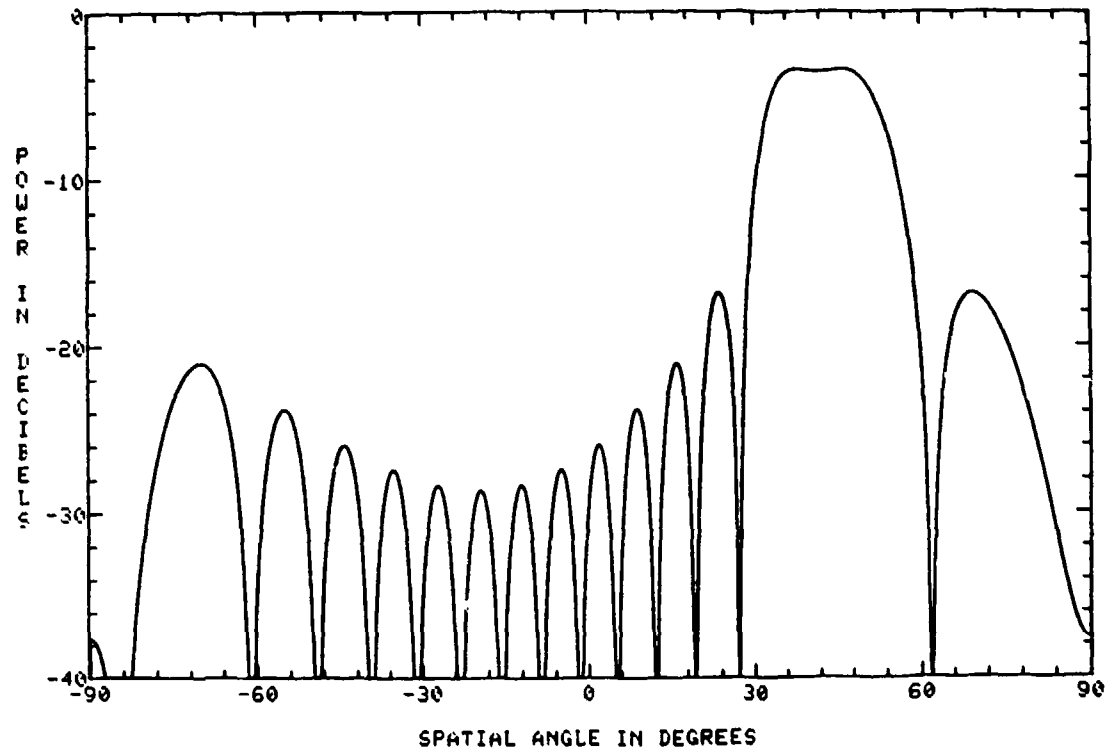

Fig. 11 — Typical AS Sector Reference beam at midband, steered to a center position of 42 degrees azimuth.

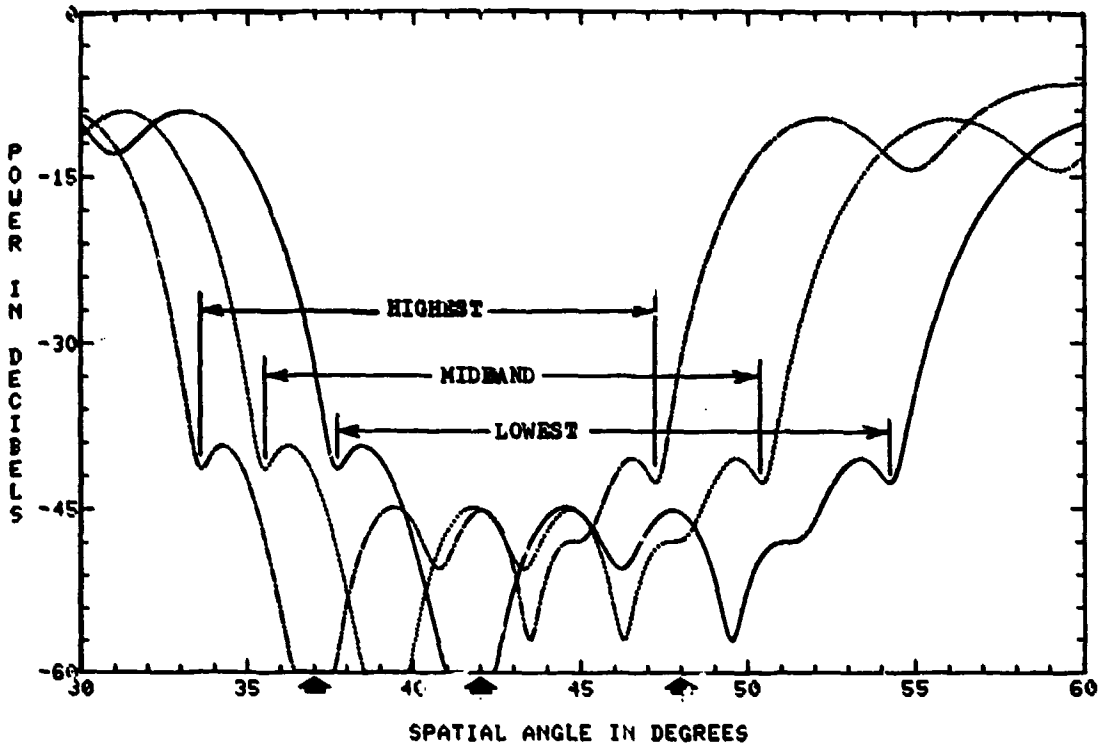

(a) Nine interferometer beams with no transversal filter (TF) present

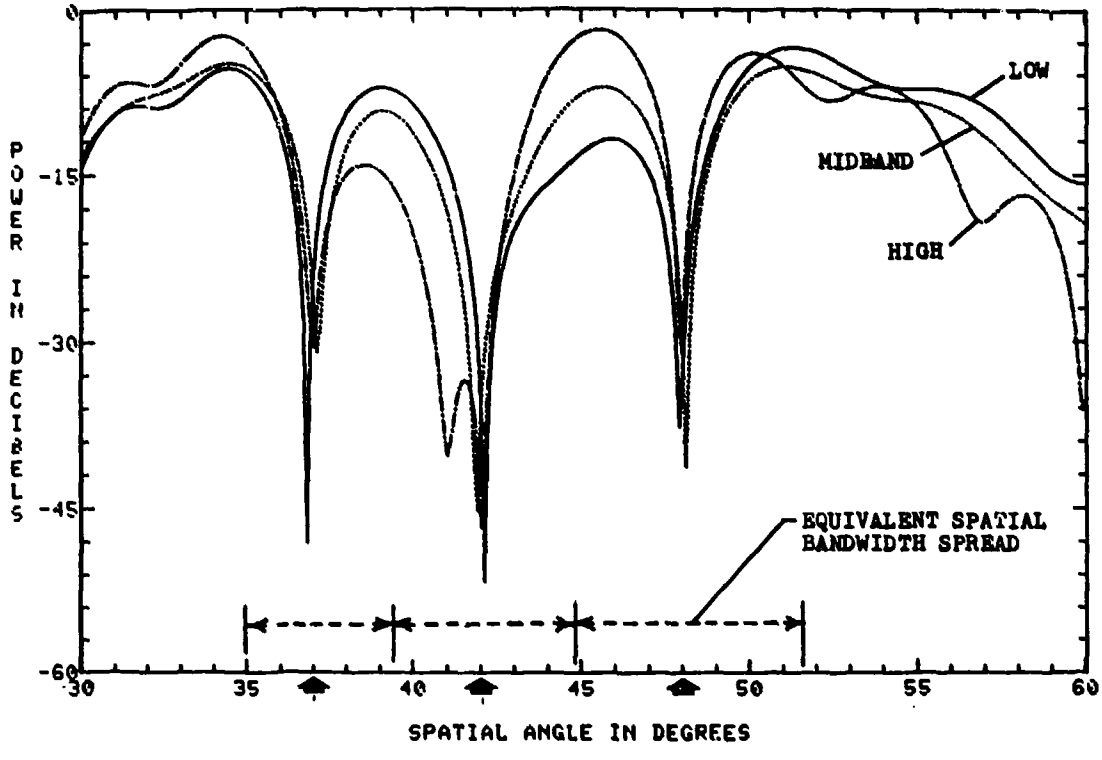

(b) Five interferometer beams with a 3-tap transversal filter on each beam

Fig. 12 — Typical adapted patterns for the case of three 16.7 dB sources of 10% bandwidth located at 37, 42, and 48 deg., with no equivalent "overlap".

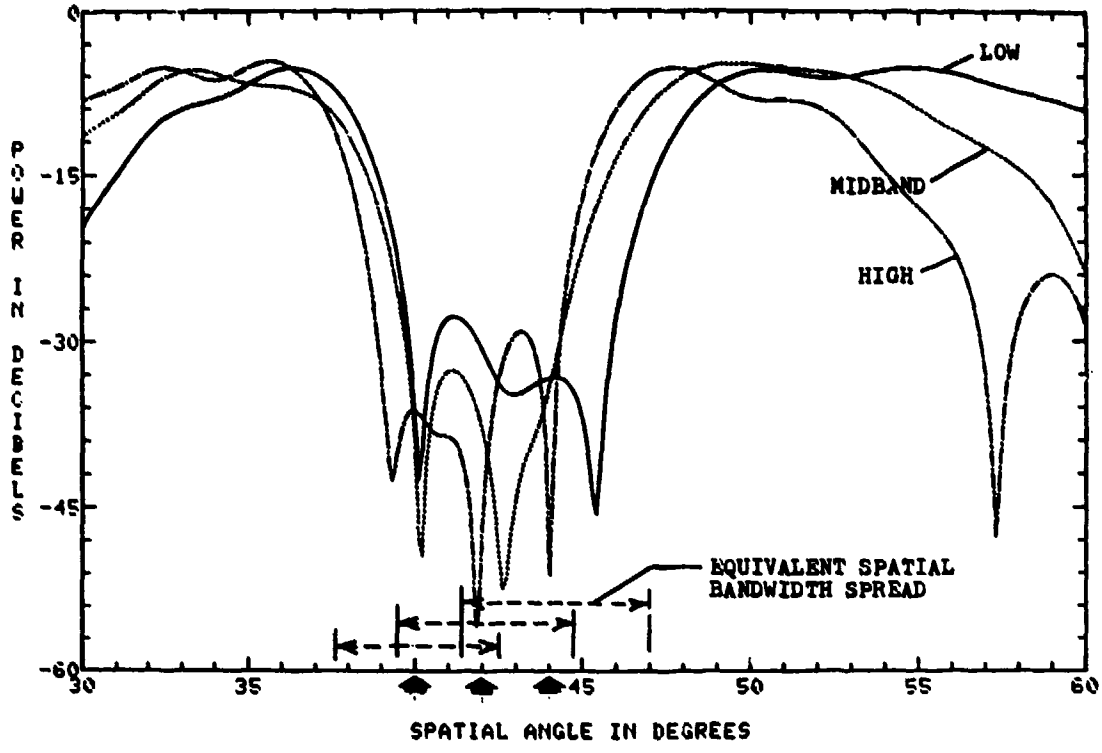

(a) AS sector reference beam steered via phase shifters

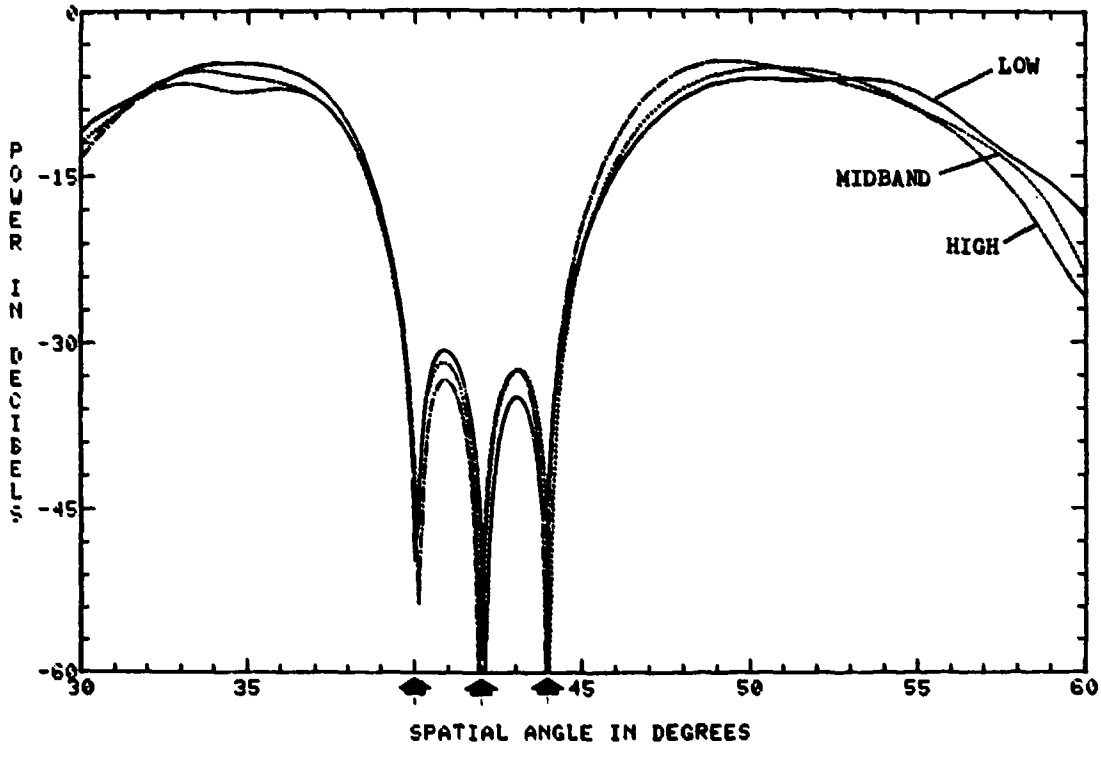

(b) AS sector reference beam steered via true time-delay

Fig. 13 — Typical adapted patterns for the case of three 16.7 dB sources of 10% bandwidth located at 40, 42, and 44 deg., with significant spatial "overlap". Five interferometer beams with a 3-tap transversal filter on each beam.

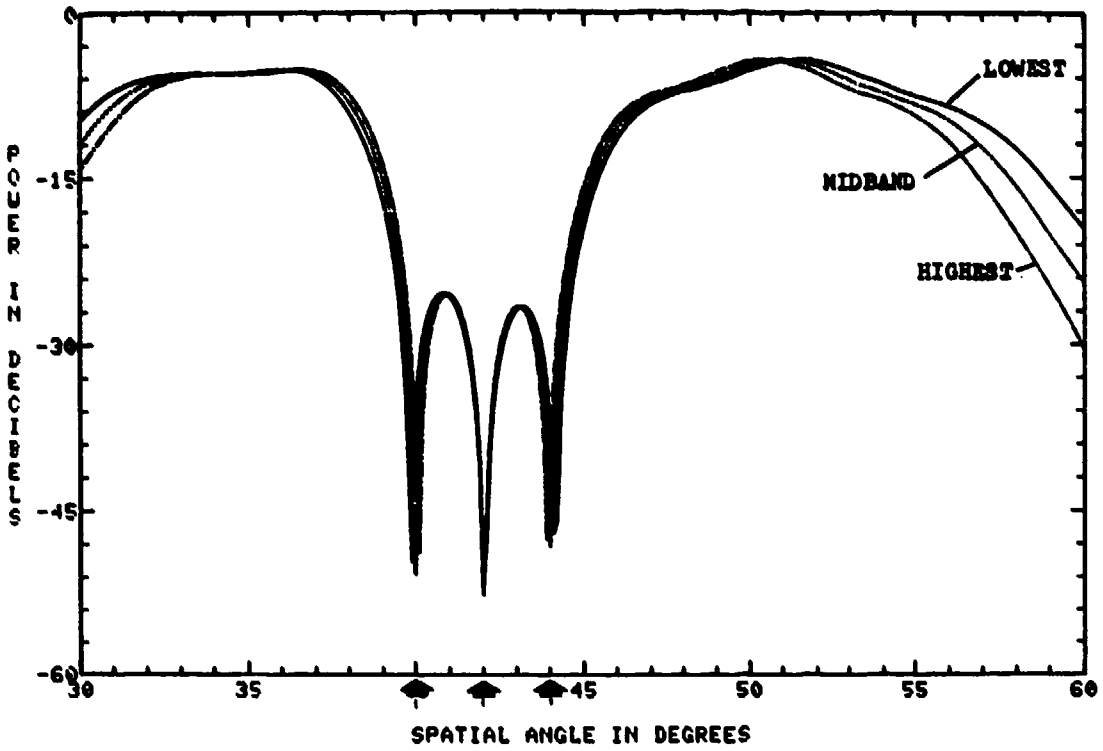

(a) Same swept-sources case as Fig. 13

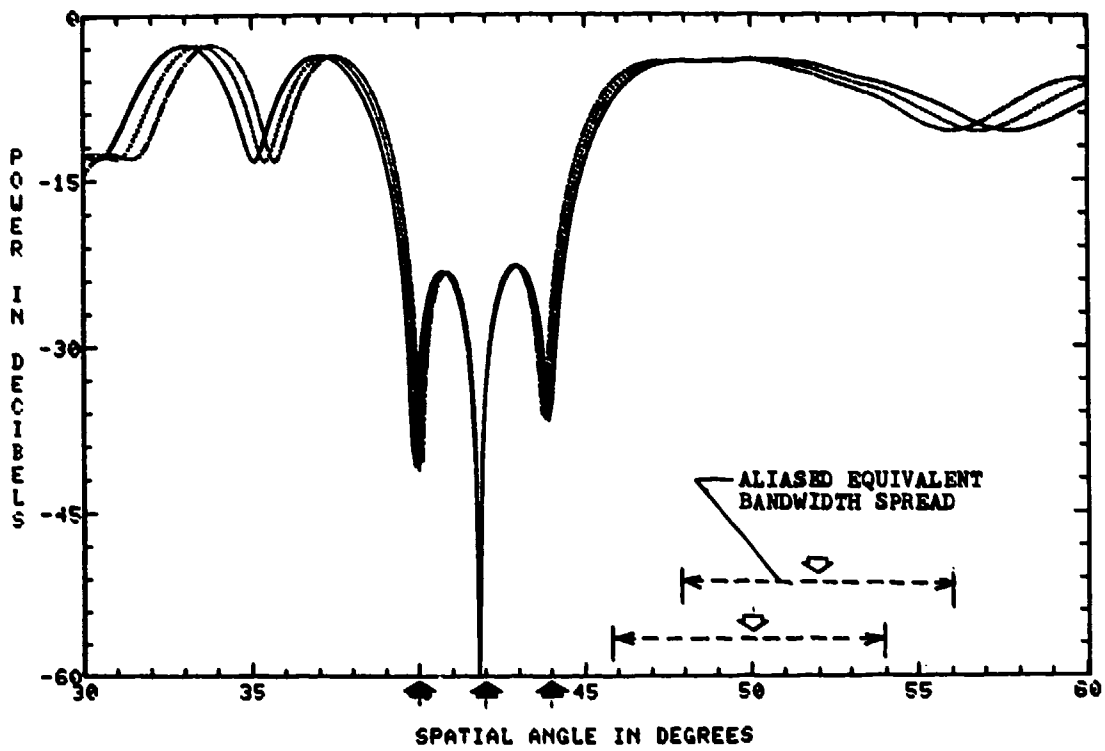

(b) Swept sources case of Fig. 13 plus two additional 20 dB sources of 10% bandwidth located at −13.5 and −12.2 deg. azimuth

Fig. 14 — Typical adapted patterns using time-delay steering on all element signals, with no transversal filters present.

APPENDIX A

Interferometer Beamformer Weights

The beamformer indicated in Fig. 9 may consist of a Butler Matrix design [A1], a Rotman lens design [A2], or any other feasible implementation [A3]. Orthogonality in the family of beams is desirable but not essential, and low sidelobe design is not required. A Rotman lens would offer the inherent advantage of incorporating true time-delay beam formation such that, in the light of the "focussed" sector discussion of Section V, it would probably be a preferred candidate in an actual system design. However, for the purposes of this report, where it was necessary to evaluate both phase-steering and time-delay steering, the Butler Matrix was a better choice.

A Butler Matrix essentially sets up a spatial discrete Fourier transform in which the transformation vector for a linear array with equal element spacing will have individual weights of the form,

$$b_{km} = \left(\frac{1}{\sqrt{K}}\right)\exp\left\{\frac{-j2\pi}{K}\left(k - \frac{K+1}{2}\right)\left(m - \frac{K+X}{2}\right)\right\} \qquad (A1)$$

where

$$X = \left(\frac{2Kd}{\lambda_o}\right)\sin\theta_b \qquad (A2)$$

m = beam index

k = element index

K = total number of elements

d = element spacing

θ_b = vernier beam adjustment angle.

For our case where K is an odd number (K=9) we chose θ_b such that X=1, and this automatically adjusts the center beam to boresight position.

It should be noted that the element weights expressed in Eq. (A1) are independent of the spacing of the elements, except for the vernier adjustment factor, X. The complete transformation matrix $\underline{B}$ then consists of K column vectors of K element weights, where the kth column vector $\underline{b}_k$ is associated with the kth beam,

$$B = \begin{bmatrix} b_{11} & b_{12} & \cdots & b_{1K} \\ b_{21} & b_{22} & & b_{2K} \\ b_{31} & b_{32} & & b_{3K} \\ \vdots & \vdots & \cdots & \vdots \\ b_{K1} & b_{K2} & & b_{KK} \end{bmatrix} \tag{A3}$$

The beamformer output vector $\hat{E}$ is expressed,

$$\underline{\hat{E}} = \underline{B}^t \underline{E} \tag{A4}$$

where $\underline{E}$ is the column vector of input signals from the array elements.

This beamformer is referred to as an "interferometer beamformer" because the input elements from the aperture are spaced $d=3\lambda_o$ apart. The implication of this wide spacing is that the cluster of beamformer beams is not unique and will replicate itself several times throughout visible space. For example, if we consider just the center beam and its boresight position, we will get its full uniform illumination peak gain at multiples of 2π interelement phasing,

$$2\pi \frac{d}{\lambda_o} \sin\theta_i = 2\pi i \tag{A5}$$

or $\sin\theta_i = i/3$ for $i = -3, -2, -1, 0, 1, 2, 3$. Therefore, the center beam replicates at the azimuth spatial angles of -90°, -41.8°, -19.5°, 0°, +19.5°, +41,8°, and +90°.

AS Sector Reference Beam

The reference beam is intended to be a spatial filter which passes the AS sector but filters out all sources that are located outside it. In attempting to approximate this ideal rectangular-shape filter without getting into sophisticated design procedures, the method of separating two sin x/x beams was utilized. It is readily shown that the element phasing required for separating the twobeams by Δ beamwidths is,

$$\phi_k = \frac{\pi\Delta}{K}\left[k - \frac{K+1}{2}\right], \tag{A6}$$

and adding the two beams results in cosine element weights W_k,

$$W_k = \frac{1}{2}\left[e^{j\phi_k} + e^{-j\phi_k}\right] = \cos\phi_k \tag{A7}$$

The array parameters chosen for this simple cosine-type weighting were K=19 elements spaced a half-wavelength apart, and a beam separation of $\Delta = 1.5$ beamwidths where a beamwidth is defined as the arc sin(2/K). By itself, this weighting produces a double-hump pattern with a 2.2 dB dip in the middle, so the end element weights were increased by +.546 to flatten and extend the central constant-gain region. Final weights obtained were: -.068, -.402, -.164, +.082, +.325, +.546, +.735, +.880, +.970, and +1.0, where +1.0 is the weight applied to the center element. Figure 11 illustrates the resultant flat-top beam at midband, steered to a center position of 42 degrees azimuth.

Figure A1 illustrates the pattern shifting that occurs at the lowest and highest frequencies within a 10% RF bandwidth under the two methods for steering the beam, phase-shifters and true time-delay. The phasing associated with the above weights for these two methods is readily determined for steering angle θ_o and half-wavelength spaced elements,

$$\text{phase shifters} = \exp(-j\,\Psi_k) \tag{A8}$$

$$\text{time delays} = \exp\left(-j(f_\ell/f_o)\Psi_k\right) \tag{A9}$$

where $\Psi_k = \pi \sin\theta_o \left[k - \frac{K+1}{2}\right]$,

f_o is the midband RF frequency and f_ℓ is the ℓth frequency within the bandwidth. The essential difference is that the phase shifter is a fixed phase setting, Ψ_k whereas time delay offers a counteracting frequency compensation to the midband setting.

A final point to be emphasized in regard to the AS sector reference beam is that its phase center is displaced $-7.5\,\lambda_o$ away from the phase center of the interferometer beams. This displacement is essential to achieving robust spatial estimation performance in our SLPF systems, because it produces a phase sensitivity to source location in a beamspace system, in addition to the amplitude sensitivity derived from beamshapes. One consequence of this displacement is that it must be taken into account in referring the AS reference beam output signal to the phase center of the interferometer beamformer. Thus, it adds an additional term to Eqs. (A8) and (A9),

$$\text{phase shifters} = \exp[-j\ (\Psi_k + \alpha)] \tag{A10}$$

$$\text{time delays} = \exp[-j(f_\ell/f_o)[\Psi_k + \alpha] \tag{A11}$$

where $\alpha = 2\pi(7.5)\sin\theta_o$.

Appendix References

A1. J. Butler, "Multiple Beam Antennas," Sanders Assoc. Internal Memo RF 3849, Jan 1960.

A2. W. Rotman and R.F. Turner, "Wide-Angle Microwave Lens for Line Source Applications," IEEE Trans. AP, Vol. 11, pp. 623-632, Nov 1963.

A3. A.W. Rudge, et al, Editors, "The Handbook of Antenna Design," Peter Peregrinus Ltd., London, UK, 1983.

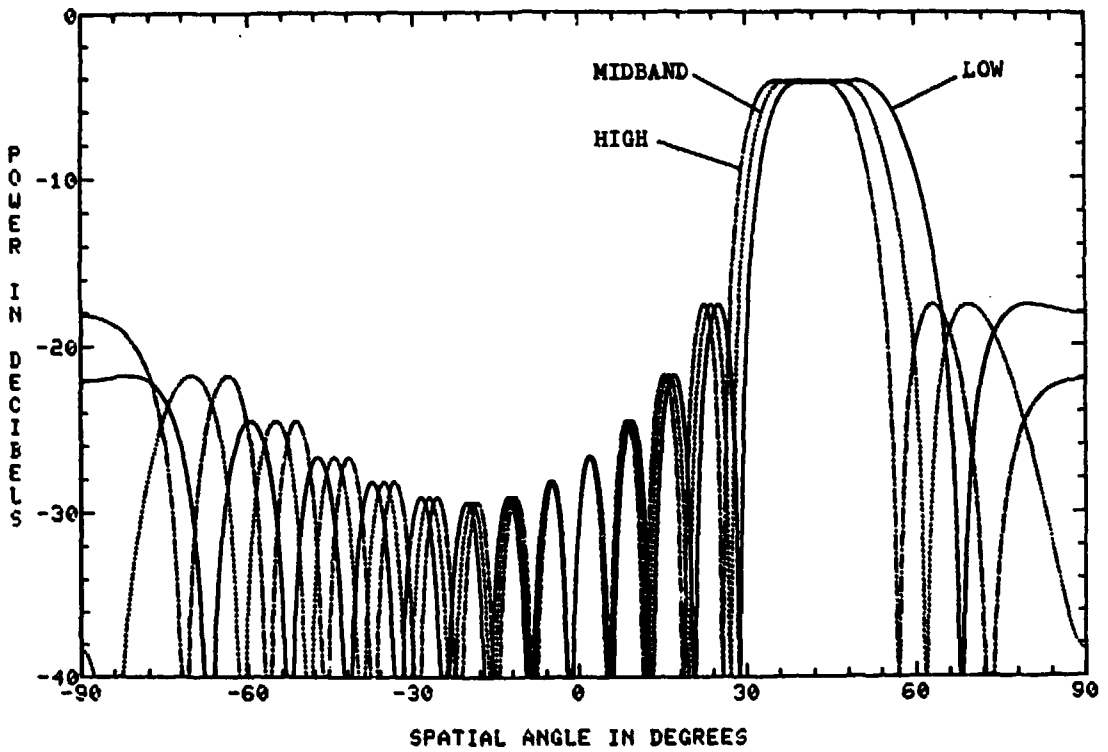

(a) Beam steered to 42 deg. azimuth via phase shifters

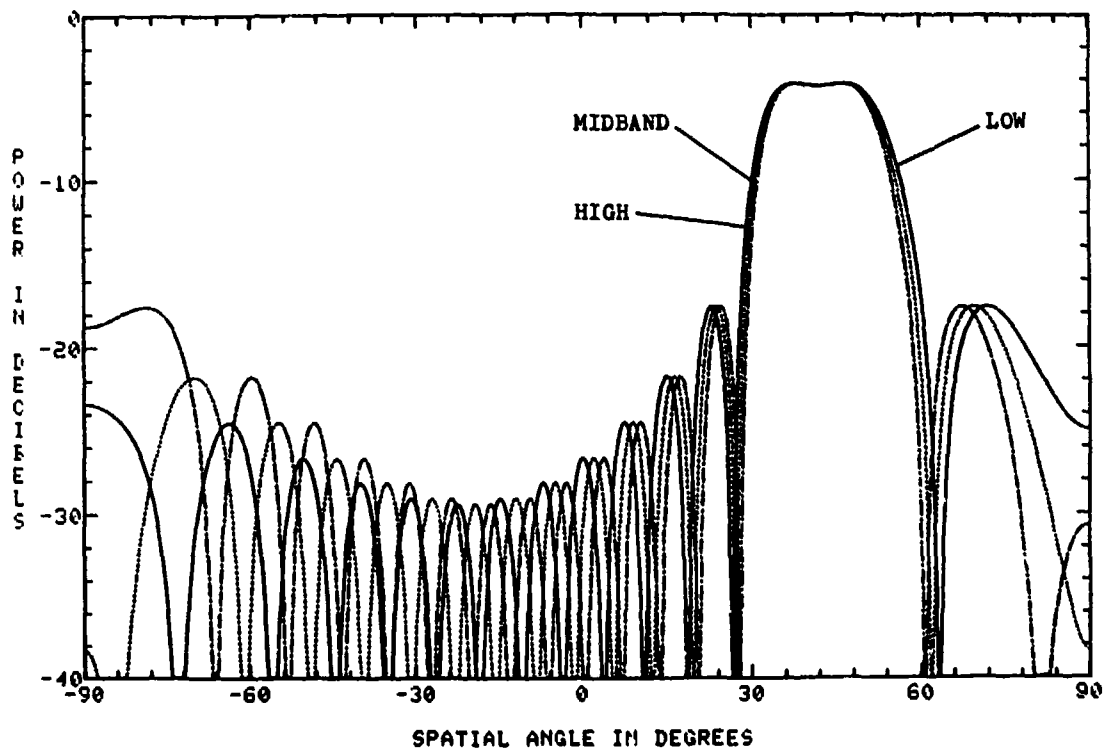

(b) Beam steered to 42 deg. azimuth via true time-delay

Fig. A1 — AS sector reference beam plotted at three frequencies within 10% RF bandwidth